9.2 RADAR CLIMATOLOGY OF TORNADOES OCCURRING IN HIGH SHEAR/LOW CAPE ENVIRONMENTS IN THE MID-ATLANTIC AND SOUTHEAST

Jason M. Davis* and Matthew D. Parker
North Carolina State University, Raleigh, North Carolina

1. INTRODUCTION

Predicting and issuing warnings for tornadoes is an important challenge for forecasters when convection occurs in high shear, low CAPE (HSLC) environments. For the purposes of this study, a HSLC environment is defined as an environment with surface-based CAPE (SBCAPE) < 500 J kg^{-1} and 0-6 km bulk shear vector magnitude > 18 m s^{-1} (35 knots). While environments with low CAPE are traditionally thought to be less favorable for deep convection, severe storms and tornadoes can and do still occur. In fact, Guyer and Dean (2010) found that almost 28 percent of all tornadoes between 2003 and 2009 occurred in environments with mixed-layer CAPE (MLCAPE) less than 500 J kg^{-1}, and Schneider and Dean (2008) noted that 16 percent of all significant (EF2 or greater) tornadoes between 2003 and 2007 occurred in similarly low CAPE environments. While Guyer and Dean (2010) found that tornadoes in low CAPE environments can occur nationwide, low CAPE tornadoes, especially significant ones, are especially concentrated in the Southeast and Mid-Atlantic regions (their Figure 1 and 2). An additional problem with HSLC tornadoes is that, given the climatological seasonal and diurnal trends in instability, they tend to occur during the cool season, when the public is less likely to expect tornadoes, and at night, when Ashley et al. (2008) found that the public has an increased vulnerability to tornadoes.

Improved understanding of the typical storm environments and radar observations associated with HSLC tornadoes is necessary for improving forecasts and warnings. A study of mesoscale environmental parameters associated with HSLC tornadoes can be found in Sherburn and Parker (2012, this volume), while this study will focus on the radar portion of this problem, on the storm scale. There are many challenges that make it difficult for forecasters to issue accurate warnings for HSLC tornadoes with sufficient lead time. Radar reflectivity and velocity structures are often less well-defined than those associated with tornadoes in environments with stronger instability, and structures can vary markedly at times from the typical structures associated with classic supercells in the Plains. Rotation may be difficult to detect, especially far from the radar, due to shallower storms and smaller mesocyclones. These may not be sampled well by the radar due to radar beam widening with range and the increase in the height of the radar beam above the Earth's surface with range. Also, numerous weak circulations may be present on the radar display, many of which are non-tornadic, making it difficult to discriminate between tornadic and non-tornadic circulations. While several case studies have been done on radar observations of HSLC tornadoes (e.g. McAvoy et al. 2000 and Lane and Moore 2006), often with a primary focus on radar reflectivity signatures, a broader, more quantitative study of a relatively large number of HSLC tornado cases has not yet been done, especially regarding radar velocity signatures.

This study seeks to find methods by which radar reflectivity and velocity signatures associated with tornadic and non-tornadic circulations can be discriminated with some skill by operational forecasters, by studying many tornadic and non-tornadic circulations from a large number of cases. A brief regional climatology and climatology of convective modes for HSLC tornadoes occurring in our domain will be presented. A climatology of azimuthal shear for tornadic and non-tornadic HSLC mesocyclones and mesovortices will be the main focus of this paper.

2. REGIONAL CLIMATOLOGY

The domain of this study encompasses 11 National Weather Service (NWS) Weather Forecast Office (WFO) County Warning Areas (CWAs) in the Southeast and Mid-Atlantic states, including portions of northern Alabama, extreme southern Tennessee, Georgia, the Carolinas, Virginia, extreme southeastern West Virginia, and Maryland. The specific WFOs and their respective CWAs that are included in this study are displayed in Fig. 1. Forecasters at these WFOs identified 107 HSLC severe weather events between January 2006 and April 2011.

Tornadoes that occurred on these days were extracted from the Storm Prediction Center's (SPC's) severe weather database, which is based on *Storm Data* and is described in Smith et al. (2012) and Thompson et al. (2012). The tornado data are subject to limitations in reporting, as discussed in Smith et al. (2012) and many previous studies. Convective environment data from the nearest 40 km grid point in the hourly SPC mesoanalysis system, as described in Thompson et al. (2012), are used to determine which tornadoes on these days occurred in a HSLC environment. The environment data are subject to potential errors in regions of strong horizontal gradients in the CAPE and shear fields, and errors in the background vertical profiles from the Rapid Update Cycle (RUC) model, as further discussed in Thompson et al. (2012).

**Corresponding author's address:* Jason M. Davis, Department of Marine, Earth, & Atmospheric Sciences, North Carolina State University, Campus Box 8208, Raleigh, NC 27695-8208. E-mail: jmdavi20@ncsu.edu.

Fig. 2 shows the number of HSLC tornadoes that occurred in each CWA in our domain for our HSLC cases between January 2006 and April 2011. Since not all CWAs are the same size, these numbers were normalized by the area of the CWA. 295 HSLC tornadoes occurred in our domain during our HSLC cases. The central and northern portions of our domain (the Mid-Atlantic states and much of the Carolinas) have a relatively uniform number of HSLC tornadoes, ranging from about 2-5 tornadoes per 10 000 square km, with the exception of the Morehead City, NC and Columbia, SC CWAs. The southern CWAs (Peachtree City, GA and Huntsville, AL) have a higher number of HSLC tornadoes per 10 000 km, along with the Columbia, SC and Morehead City, NC CWAs. The Huntsville, AL CWA has an anomalously high 27 HSLC tornadoes per 10 000 square km. The tendency for more HSLC tornadoes to occur in the southern portion of the domain is somewhat surprising given that instability typically decreases to the north, but it is hypothesized that given high shear, perhaps there are more convective days occurring with low CAPE in the southern portion of the domain and no instability in the central and northern portions of the domain.

3. CLIMATOLOGY OF CONVECTIVE MODES

The convective mode for each tornado (filtered to only include the strongest tornado that occurred in each 40 km grid cell during each hour) was also acquired from the SPC database. Convective mode data were available for 224 of the 295 HSLC tornadoes. The convective mode classification method is described in Smith et al. (2012). Tornadoes were classified by Smith et al. (2012) as either supercellular or non-supercellular, depending on whether their parent storm contained an area of rotation that met Smith et al. (2012)'s mesocyclone criteria. Supercells were sub-classified as discrete supercells, supercells in clusters, and supercells in lines. Non-supercellular tornadoes were classified as quasi-linear convective system (QLCS) tornadoes if their parent storm met Smith et al. (2012)'s QLCS criteria. Importantly, tornadoes associated with supercells embedded in a system meeting QLCS criteria were given the "supercell in line" classification, not the QLCS classification. For our analysis, almost all HSLC tornadoes fell into either the supercell or QLCS classification, so the very few non-supercellular tornadoes not associated with a QLCS were designated by us as "other".

The distribution of convective modes for the 224 HSLC tornadoes with convective mode data is shown in Fig. 3, along with the convective mode distribution of all (regardless of their associated CAPE and shear values) 10 724 tornadoes that occurred nationwide between 2003 and 2011. The majority of HSLC tornadoes were associated with supercells, but this percentage was slightly less (6%) than for all tornadoes. The percentage of HSLC QLCS tornadoes is more than 15% greater than the percentage of QLCS tornadoes for all tornadoes. When considering only supercell and QLCS tornadoes and not tornadoes in the "other" category, it is especially clear that the relative frequency of QLCS tornadoes is greater and the relative frequency of supercell tornadoes is less for HSLC tornadoes compared to all tornadoes.

Fig. 3 also shows the distribution of the three supercell sub-classification types for HSLC tornadoes and all tornadoes. Interestingly, only 25% of the HSLC supercell tornadoes were from discrete supercells compared to 40% of all supercell tornadoes. Meanwhile 75% of the HSLC supercell tornadoes were from non-discrete supercells (supercells in clusters and supercells in lines) compared to 60% of all supercell tornadoes. The reasons for an enhanced relative frequency of non-discrete supercells and QLCSs in HSLC environments are unclear. It is possible that perhaps storms in environments with low instability need a greater degree of external forcing in order to survive, resulting in discrete supercells being less favored. Another possibility is that HSLC environments tend to have more widespread convection than the typical supercell environment in the Plains, possibly due to a typically weaker cap and stronger synoptic-scale forcing for ascent promoting upscale growth. These hypotheses cannot be tested based on the data presented here, but they are an area of interest for modeling and observational studies in the future.

4. CLIMATOLOGY OF MESOCYCLONES AND MESOVORTICES

a. Motivation

While operational Doppler radars rarely can resolve the circulation of the tornado itself, due to the relative sizes of the radar beamwidth and tornado, forecasters often consider low-level rotation associated with the parent mesocyclone/mesovortex when issuing tornado warnings. This can pose a challenge as both tornadic and non-tornadic supercells can have low-level mesocyclones (Trapp 1999, Trapp et al. 2005). There are still many aspects of tornadogenesis that are not fully understood, and many storm-scale processes that currently cannot be well-observed operationally. Environmental factors are also important, but forecasters cannot always determine if a storm is in a favorable environment for tornadoes. Therefore, studying the strength of the radar-observed rotation in mesocyclones and mesovortices, and how this varies both over time and vertically is important, so that factors that can discriminate between tornadic and non-tornadic storms, if any, can be determined. It is also important to attempt to determine what the potential lead time is for HSLC tornadoes, and which radar velocity information is most important for forecasters to focus on.

Doppler radars only measure the component of the wind that is parallel to the radar beam, the radial velocity. Therefore, rotation is not directly observed by the radar; rotation is inferred by strong horizontal shear, a strong gradient in radial velocity in the azimuthal direction. Previous papers have studied azimuthal shear and rotational velocity associated with tornadoes typically in one of two ways. Some studies have used a case study type of approach, manually calculating timeseries of azimuthal/rotational shear or rotational velocity for a handful of tornadic storms (e.g. Funk et al. 1999, Atkins et al. 2004, Atkins et al. 2005, Schumacher and Boustead 2011). Others have focused on azimuthal shear at one point in time for the purposes of developing tornado and mesocyclone detection algorithms (e.g. Stump et al. 1998). These algorithms can be used to develop mesocyclone climatologies (e.g. Wood et al. 1996, Trapp 1999, Jones et al. 2004, Trapp et al. 2005) in order to determine the percentage of tornadic mesocyclones, for example. In this study, we seek to study *changes in azimuthal shear over time for a composite of a large number of cases*, which requires the development of an automated method for tracking, not just detecting, mesocyclones and mesovortices (hereafter more generically referred to as "vortices"). The unique aspect of this study is the ability to look at temporal and vertical changes in vortex strength for a large number of cases. This portion of the study is an area of ongoing research, so the methods and results should be considered preliminary.

b. Methods

NEXRAD Level II radar data were downloaded from the NCDC archive for all of our HSLC cases that occurred after the WSR-88D radars in our region were upgraded to "super-resolution" (Wood et al. 2001) in the summer of 2008. This was due to concerns regarding the potential inconsistency of comparing azimuthal shear calculated from higher resolution velocity data with azimuthal shear calculated from the previously available coarser "legacy resolution" velocity data. Therefore, the time range used in this portion of the study is necessarily shorter than what was used in the regional climatology and convective modes climatology portions of the study. The time frame for this portion of the study includes 151 HSLC tornadoes that occurred between fall 2008 and spring 2011. The radar data were initially processed using the Warning Decision Support System-Integrated Information (WDSS-II; Lakshmanan et al. 2007) application. Automated WDSS-II algorithms were used to remove non-meteorological echoes from the radar reflectivity data and dealias the radial velocity data.

Azimuthal shear was calculated by WDSS-II using the two-dimensional linear least squares derivative technique developed by Smith and Elmore (2004). This technique is more tolerant of noisy data and less dependent on the azimuthal offset of the vortex relative to the radar beam (but still dependent on range from the radar) than traditional rotational shear calculations that only use velocity data from two points. Once a polar, gridded azimuthal shear field was generated in WDSS-II, with the same resolution as the raw super-res velocity data, it was interpolated into a 0.01 degree latitude by 0.01 degree longitude Cartesian grid. This may cause some smoothing of the azimuthal shear data, and in the future some experimentation using a higher resolution for the Cartesian grid may be done. An example of radial velocity and azimuthal shear for a vortex is shown in Fig. 4.

Both tornadic and non-tornadic vortices were tracked. Tornadic vortices were initially tracked using the tornado touchdown points from the SPC database as a starting point. Since some vortices could potentially produce multiple tornadoes, a check was performed to remove duplicate tracked vortices from the dataset, and only the vortex track associated with the first tornado produced by the vortex was included in further analysis. Non-tornadic vortices were determined by downloading the text data for all HSLC tornado warnings issued for our HSLC cases from the Iowa Environmental Mesonet archive (http://mesonet.agron.iastate.edu/archive/). Vortices associated with these warnings were tracked, and if no tornadoes were reported within a 0.5 degree latitude by 0.5 degree longitude box centered on each tracked position of the vortex, within one hour, that vortex was determined to be a non-tornadic vortex, associated with an unverified tornado warning. This method does likely eliminate some false alarm warnings in cases where a non-tornadic vortex tracked in close proximity to a tornado from a different vortex. However, it helps to account for small spatiotemporal errors in the tornado database by removing tornado warnings that occurred in proximity to a tornado track. It also removes warnings issued for a vortex that was tornadic at other stages during its lifetime. It is possible, however, that a tornado could have occurred with the vortex but not have been reported, due to the limitations of the tornado record.

Vortices were tracked by their local maximum in azimuthal shear for any radar elevation scan in the 0-2 km MSL layer. This method was used rather than only using the radar base scan in order to potentially track vortices before they developed substantial rotation at the lowest elevation scan. The vortex position was initially found by searching for the location of the maximum in azimuthal shear within a 0.1 degree latitude by 0.1 degree longitude square centered on the tornado touchdown point (for tornadic vortices) or the storm location listed in the tornado warning (for non-tornadic vortices). This search was performed on the closest radar's volume scan that immediately preceded the tornado touchdown time/false alarm warning issuance time. This somewhat broad initial search radius accounts for some small potential errors in tornado/warning location/time and offsets between the tornado touchdown/warning issuance time and the time of the preceding volume scan. If azimuthal shear values greater than 0.006 s^{-1} (a subjectively determined noise threshold) could not be found within this box, the tornado/warning was omitted from the study, due to any rotation being extremely weak or a potential large error in the tornado touchdown time/position or storm position included in the warning.

The vortex is then tracked backwards and forwards in time. This process is summarized by the flow chart in Fig. 5. The basic philosophy behind this tracking method is to extrapolate the vortex position from an estimated vortex motion, but then search for the actual vortex position within a search radius defined by an estimate of the uncertainty associated with the vortex motion estimate. It incorporates information from the pre-existing operational mesocyclone detection and storm tracking algorithms (algorithm text data were downloaded from the NCDC Severe Weather Data Inventory at http://www.ncdc.noaa.gov/swdiws) to narrow the search radius when possible. However, it also is flexible in order to account for cases that may not trigger these algorithms, or for cases in which using the algorithms alone does not give an accurate track. This tracking method was rigorously tested through comparing the vortex tracks from the automated method with manually determined vortex tracks for multiple cases. As with all automated algorithms, it cannot be expected to be perfect. It will struggle with vortices located close together, or cases when one vortex dissipates and another reforms within one volume scan. However, the results should give an overall picture of what a forecaster would see over time in the radar velocity data.

Initially, the vortex is tracked backward in time, in an iterative process. A first guess position of the vortex during the previous volume scan is first estimated based on an estimate of vortex motion. The estimated vortex motion over the first two backward timesteps is initially taken to be the storm motion vector associated with the nearest storm to the vortex, based on output from the Storm Cell Identification and Tracking (SCIT) algorithm (Johnson et al. 1998). Later on in the process, after three vortex positions have been determined, an extrapolation of the three previously found vortex positions is used instead. Using the estimated vortex motion, the position of the vortex is predicted, and then an azimuthal shear maximum is searched for within a search radius defined by the typical uncertainty in the vortex motion vector (Fig. 6).

Through rigorous testing, it was determined that a search radius allowing for a vortex motion uncertainty of 18 m s^{-1} produced the most accurate tracks when using a vortex motion estimate from the SCIT algorithm (during the first two timesteps), and an uncertainty of 9 m s^{-1} was used when the vortex motion estimate was from an extrapolation of previously found vortex positions. This difference is due to possible error in the SCIT storm motion vector, while an extrapolated motion from previously found vortex positions has higher confidence. For a typical radar volume scan time of 280 s, this corresponds to search radii of about 5 km for the 18 m s^{-1} motion uncertainty, and 2.5 km for the 9 m s^{-1} motion uncertainty. A smaller search radius for the azimuthal shear maximum was used if a mesocyclone found by the Mesocyclone Detection Algorithm (MDA) fell within the initial search radius (using the closest mesocyclone to the predicted vortex position if multiple mesocyclones fell within the initial search radius). Also, if a mesocyclone with the same identification code is found by the MDA within the search radius for at least two consecutive volume scans (since the MDA is sometimes able to track vortices), its position is automatically used rather than searching for an azimuthal shear maximum. Once an azimuthal shear maximum was found, the process repeats itself for the next volume scan back in time.

The vortex is tracked backward and forward in time from its initial point in this manner until the azimuthal shear maximum falls below a certain threshold. This threshold is initially 0.006 s^{-1}, which was the lowest azimuthal shear value at which the weakest tornadic vortices could be detected, but is raised to 0.008 s^{-1} if consistently higher values of azimuthal shear are found. This is because it was easier to distinguish vortices from background noise in the velocity field with this higher threshold. Once a preliminary vortex track is found, the vortex tracking algorithm makes a second pass and again searches for the azimuthal shear maximum within a 0.04 degree by 0.04 degree box centered on the preliminary vortex positions. This accounts for cases when the tracking algorithm may not have found the exact center location or the highest azimuthal shear values associated with the vortex. This is typically a wider search radius than what is used in the first pass, so it is possible that higher azimuthal shear values from a different vortex may occasionally be found. However, if wider search radii were used in the first pass, the detected vortex track would be more likely to diverge from the actual vortex track. This method compromises between following the general track of the vortex and ensuring that the highest azimuthal shear values associated with the vortex are found.

The positions used in the second pass are then used for a third pass, when the azimuthal shear values used for analysis are actually recorded. At the base scan, the maximum azimuthal shear value within a 0.04 degree by 0.04 degree box centered on the vortex position found in the second pass is recorded. For higher tilts, the vortex position is likely downstream from the position found at the base scan, due to advection of the storm during the volume scan and a possible tilt of the vortex with height. Therefore, the vortex positions used in the higher tilts are determined using a linear interpolation between the vortex position at the current volume scan and the next volume scan, which accounts for advection of the vortex between elevations scans, but not storm tilt.

c. Results

83 unique tornadic vortices and 84 unique non-tornadic vortices have been successfully tracked (Fig. 7). Additional vortices may be included in future work. Due to radar sampling limitations, azimuthal shear for two identical vortices will be lower for the vortex that is farther from the radar (Newman et al. 2012). This is due to radar beam geometry. The radar beam widens with

range. Therefore, the circulation is not sampled as well at far ranges, as fewer radials cross the circulation. This results in some smoothing of the velocity field due to an averaging of the returned velocities across a larger area (beam filling), and consequently results in smoothing of the azimuthal shear field. This effect is greater for circulations with smaller diameters, and small circulations at far ranges from the radar cannot be sampled by the radar at all. This range dependence means that strong rotation far from the radar may have smaller azimuthal shear than weaker rotation close to the radar. Newman et al. (2012) developed an algorithm that attempts to correct azimuthal shear values for this type of range dependence; this range-corrected azimuthal shear field will be studied in future work but will not be included in this analysis. An additional factor that can cause range dependence in azimuthal shear is the increase in height of the radar beam with range. This means that the lowest radar elevation scan may overshoot rotation occurring at low levels, and could especially be a problem for shallow HSLC vortices.

Due to the range dependence of azimuthal shear, vortices were sorted into three separate bins based on the distance of the tornado/false alarm warning from the closest radar. Fig. 8 shows the number of tornadic and non-tornadic vortices that fall into these bins, which are 0-50, 50-100, and 100-150 km from the nearest radar. A similar range distribution was found for tornadic and non-tornadic vortices, with about 20 vortices in the 0-50 km and 100-150 km bins, and about 50 vortices in the 50-100 km bin. The high number of samples in the 50-100 km bin suggests that of the following results, the results for this bin have the most confidence.

Fig. 9 shows a composite timeseries of azimuthal shear at the 0.5 degree elevation scan for the tornadic vortices within 50 km of the nearest radar in a tornado-relative time-coordinate system. The center of the *t* axis (the horizontal axis) is the volume scan immediately prior to tornado touchdown for each tornado, with *t* values greater than or less than zero corresponding to each volume scan after or before tornado touchdown, respectively. Since different vortices could be tracked for different amounts of time, the number of samples for each *t* point varies, as not every vortex existed or could be tracked forward and backward to every *t* point. As would be expected, the number of vortices that could be tracked to volume scans farther backward and forward from the tornado touchdown decreases over time. In this figure, all trackable vortices exist at the volume scan prior to tornado touchdown, and most vortices exist for a couple previous volume scans. A little more than half of the vortices were present at the fifth volume scan prior to the tornado; for a typical volume scan time of about 5 minutes this corresponds to about 25 minutes prior to the tornado. The existence of most trackable vortices for a couple volume scans prior to the tornado is important for forecasters, indicating the potential for lead time in a tornado warning.

Median azimuthal shear values are plotted for only the vortices that existed at each *t* point, and are only plotted if at least 5 vortices existed at that *t* point. For volume scans farther backward or forward in time, the decrease in the number of samples means that apparent trends in median azimuthal shear at those times may be due to noise. At least five of the vortices could be tracked backwards in time almost 10 volume scans (approximately 50 minutes). Looking at the five volume scans leading up to the tornado, an upward trend in median azimuthal shear is found at the base scan, indicating a tendency for vortex strengthening leading up to the tornado as would be expected. A downward trend is found after the tornado. Median azimuthal shear values are above 0.01 s^{-1} for a long period of time, and at one volume scan prior to tornado touchdown even the 25th percentile is above 0.01 s^{-1}. Overall, these results indicate that meaningful rotation could be detected for most tornadic vortices that were close to a radar before the tornado occurred.

Moving farther away from the radar, Fig. 10 shows a similar plot for tornadic vortices located 50-100 km from the nearest radar. Similarly, roughly half of the vortices could be tracked five volume scans prior to tornado touchdown, but not all vortices can be tracked more than 1-2 volume scans prior to tornado touchdown. A slight upward trend may exist prior to the tornado, but this is less clear. Overall median azimuthal shear values appear relatively flat. Median azimuthal shear values are greater than 0.01 s^{-1} prior to the tornado, but are weaker than for the tornadic vortices less than 50 km from the nearest radar.

For tornadoes greater than 100 km from the nearest radar, Fig. 11 shows that again roughly half of the vortices can be tracked at least five volume scans prior to tornado touchdown. Interestingly, there is a downward trend in median azimuthal shear leading up to tornado touchdown. This combined with azimuthal shear values below 0.01 s^{-1} at the volume scan immediately prior to tornado touchdown suggests that these vortices are probably not being well-sampled by the radar.

Most of the non-tornadic vortices within 50 km of the radar could be tracked five volume scans prior to the tornado warning, in this composite timeseries (Fig. 12) plotted in a warning issuance-relative time coordinate system. There was a sudden increase in median azimuthal shear values in the volume scan immediately prior to the issuance time of the false alarm warning compared to the previous volume scan, but then the median azimuthal shear values level off and decrease somewhat. A comparison with the tornadic vortices (Fig. 13) indicates that the azimuthal shear values for the non-tornadic vortices tended to be lower than for the tornadic vortices. The median azimuthal shear value for the non-tornadic vortices is usually well below the 25th percentile for the tornadic vortices, and the median azimuthal shear value for the tornadic vortices is typically close to or above the 75th percentile for the non-tornadic vortices. Also, the median values of azimuthal shear for the non-tornadic vortices at the time of the warning issuance are closer to the 25th percentile than the 75th percentile, indicating a non-Gaussian distribution with mostly very weak azimuthal shear values and a few stronger outliers. It should be noted that comparing plots of the tornadic vortices in a tornado-relative time coordinate system and the non-tornadic vortices in a warning-issuance relative time coordinate system may not be entirely realistic, since ideally a warning would be issued prior to the occurrence of a tornado. However, the tornadic vortices still appear to be stronger than the non-tornadic vortices after the time of warning issuance for the non-tornadic vortices. There is more overlap five volume scans after warning issuance, but the sample size for the non-tornadic vortices is fairly small at this point.

Only about 40 percent of the non-tornadic vortices between 50 and 100 km from the radar could be tracked five volume scans prior to the tornado warning (Fig. 14). This is a smaller percentage than for the tornadic vortices that may imply shorter vortex lifetimes, but this is not entirely clear and will be a subject of future work. There is a slight upward trend in median azimuthal shear leading up to the warning issuance time, when the median briefly reached 0.01 s^{-1}, and then a slight downward trend. Comparing the non-tornadic with the tornadic vortices (Fig. 15) indicates that median azimuthal shear is greater for the tornadic vortices, but there is a lot of overlap as the median of each respective population is between the 25th and 75th percentiles of the other.

Most of the non-tornadic vortices more than 100 km from the radar could not be tracked more than one or two volume scans forward and backward from the warning issuance time, indicating short-lived or not well-sampled vortices (Fig. 16). A slight downward trend in median azimuthal shear is observed throughout. A comparison with the tornadic vortices at this range (Fig. 17) indicates little difference in median azimuthal shear values between the two populations, but the tornadic vortices appear to typically have a longer trackable lifetime.

Looking at the vertical structure of tornadic and non-tornadic vortices also shows some interesting results. Azimuthal shear spikes above 0.01 s^{-1} at all elevation scans up to the 3.1 degree elevation scan for tornadic vortices within 50 km of the radar at the volume scan prior to the tornado (Fig. 18; the 1.3 degree and 2.4 degree elevation scans were omitted for clarity). Upward trends leading up to the tornado are noted in these elevation scans, with downward trends afterwards. Median azimuthal shear values at the time of the tornado are highest at the base scan, while they are fairly similar at the 0.5, 0.9, and 1.8 degree elevation scans at the times leading up to the tornado. This shows that elevated values of azimuthal shear can typically be found at higher tilts for these vortices, not just at the base scan.

Interestingly, for the non-tornadic vortices within 50 km of the nearest radar (Fig. 19), while median azimuthal shear is fairly weak at the base scan at the time of warning issuance, it is larger at the higher elevation scans. Median azimuthal shear is even above 0.01 s^{-1} at the 1.8 degree and 3.1 degree elevation scans, closer to the median values at the base scan for tornadic vortices at this range. The median values of azimuthal shear at higher tilts decrease after warning issuance time, while median azimuthal shear at the base scan increases somewhat, but not to the values found aloft at warning issuance time.

For tornadic vortices 50-100 km from the nearest radar, overall median azimuthal shear is lower at higher tilts than for tornadoes less than 50 km from a radar (Fig. 20). Azimuthal shear greater than 0.01 s^{-1} can only be found as high as the 1.3 degree tilt. This is likely due to the fact that the higher tilts are sampling the vortex at a higher altitude compared to the vortices closer to the radar, and are probably overshooting the vortex. Median azimuthal shear values at the 0.5 degree and 0.9 degree tilt are fairly similar, with possibly slight upward trends leading up to the tornado.

The non-tornadic vortices between 50-100 km from a radar do not show the interesting structure of higher azimuthal shear at higher tilts that was found for the non-tornadic vortices close to the radar (Fig. 21). Instead, the same overall pattern that existed for the tornadic vortices at this range exists, except the median azimuthal shear values are shifted downward. Azimuthal shear at higher tilts for tornadic and non-tornadic vortices more than 100 km from a radar tended to be weak and is not shown here, again showing the difficulty in adequately sampling vortices at longer ranges from the radar.

5. CONCLUSIONS

Issuing accurate tornado warnings in HSLC environments continues to be challenging. This study has shown that a substantial number of HSLC tornadoes occurred in our domain during the time period studied. The tendency for a lower relative frequency of discrete supercell tornadoes and a higher relative frequency of QLCS tornadoes help to illustrate one factor of this problem. The QLCS and non-discrete supercell convective modes typically are more difficult to issue accurate warnings for, and much is still not known about QLCS mesovortices and their role in tornadoes (e.g. Trapp and Weisman 2003, Weisman and Trapp 2003, Atkins and St. Laurent 2009a and 2009b, Schenkman et al. 2012).

Besides convective mode, the tendency for narrower and shallower vortices in HSLC storms and the subsequent effects on radar sampling also results in a challenge. A climatology of mesocyclones/ mesovortices shows that azimuthal shear can discriminate between tornadic vortices and non-tornadic vortices, both at the base scan and also aloft, within 50 km of a radar. Here, the tornadic vortices tend to have fairly strong azimuthal shear values. However, azimuthal shear does not discriminate very well as range from the radar increases. This is likely due to the range dependence of azimuthal shear. Newman et al. (2012) developed a method to range-correct azimuthal shear, and this method will be tested in future work. However, this method only works if a vortex is partially resolvable by the radar, which is not the case if it is too narrow, or if the vortex is below the radar horizon. Additionally, some of the differences between vortices within 50 km of the nearest radar and vortices 50-100 km from the nearest radar may be due to differences in sample size.

The data suggest that in some cases tornadic vortices may be longer lived than non-tornadic vortices as may be expected, but there is some conflicting evidence that needs to be explored further. Estimates of lifetime for each vortex, such as the time that the vortex has azimuthal shear above a certain threshold value, will be done in future work. Additionally, future work will be done to determine if tornadic vortices are deeper than non-tornadic vortices. Differences between supercell and QLCS vortices will also be explored, along with overall more quantitative analyses of the features discussed in this paper.

The overall goal of this study is to find ways to improve tornado warnings, so future work will focus on applying this research to operations. This study also presents a new automated method for creating a climatology of azimuthal shear for tornadic and non-tornadic vortices, and comparisons of these results with tornadoes in higher CAPE environments would be of interest. This study also focused primarily on features in radial velocity; future work should also study features in radar reflectivity associated with HSLC tornadoes as well.

Acknowledgements: This research was supported by NOAA grant NA10NWS4680007, and the first author also received funding from the AMS/NASA Earth Science Graduate Fellowship. Numerous discussions with the collaborating NWS WFO's in this Collaborative Research and Training (CSTAR) project were very beneficial, and we would like to especially thank Justin Lane, Patrick Moore, Jonathan Blaes, and Hunter Coleman for their work and input. We would also like to thank Andy Dean from the Storm Prediction Center for his help with data acquisition, and the members of the Convective Storms Group at NC State for their feedback and support.

6. REFERENCES

Ashley, W.S., A. J. Krmenec, and R. Schwantes, 2008: Vulnerability due to nocturnal tornadoes. *Wea. Forecasting*, **23**, 795–807.

Atkins, N.T., J.M. Arnott, R.W. Przybylinski, R.A. Wolf, and B.D. Ketcham, 2004: Vortex structure and evolution within bow echoes. Part I: Single-Doppler and damage analysis of the 29 June 1998 derecho. *Mon. Wea. Rev.*, **132**, 2224–2242.

Atkins, N.T., C.S. Bouchard, R.W. Przybylinski, R.J. Trapp, and G. Schmocker, 2005: Damaging surface wind mechanisms within the 10 June 2003 Saint Louis bow echo during BAMEX. *Mon. Wea. Rev.*, **133**, 2275–2296.

Atkins, N.T., and M. St. Laurent, 2009: Bow echo mesovortices. Part I: Processes that influence their damaging potential. *Mon. Wea. Rev.*, **137**, 1497–1513.

Atkins, N.T., and M. St. Laurent, 2009: Bow echo mesovortices. Part II: Their genesis. *Mon. Wea. Rev.*, **137**, 1514-1532.

Funk, T.W., K.E. Darmofal, J.D. Kirkpatrick, V.L. DeWald, R.W. Przybylinski, G.K. Schmocker, and Y.J. Lin, 1999: Storm reflectivity and mesocyclone evolution associated with the 15 April 1994 squall line over Kentucky and southern Indiana. *Wea. Forecasting*, **14**, 976–993.

Guyer, J. L., and A. R. Dean, 2010: Tornadoes within weak CAPE environments across the continental United States. Preprints, *25th AMS Conf. on Severe Local Storms,* Denver, CO, 1.5.

Johnson, J. T., P.L. MacKeen, A. Witt, E.D. Mitchell, G.J. Stumpf, M.D. Eilts, and K.W. Thomas, 1998: The Storm Cell Identification and Tracking algorithm: An enhanced WSR-88D algorithm. *Wea. Forecasting*, **13**, 263–276.

Jones, T.A., K.M. McGrath, and J.T. Snow, 2004: Association between NSSL Mesocyclone Detection Algorithm-detected vortices and tornadoes. *Wea. Forecasting*, **19**, 872–890.

Lakshmanan, V., T. Smith, G. Stumpf, and K. Hondl, 2007: The Warning Decision Support System–Integrated Information. *Wea. Forecasting*, **22**, 596–612.

Lane J.D., and P.D. Moore, 2006: Observations of a non-supercell tornadic thunderstorm from terminal Doppler weather radar. Preprints, *23rd Conf. Severe Local Storms*, St. Louis, MO., P4.5.

McAvoy, B. P., W. A. Jones, and P. D. Moore, 2000: Investigation of an unusual storm structure associated with weak to occasionally strong tornadoes over the eastern United States.

Preprints, 20^{th} *Conf. on Severe Local Storms*, Orlando, FL, 182-185.

Newman, J., V. Lakshmanan, P. Heinselman, M. Richman, and T. Smith, 2012: Range-Correcting Azimuthal Shear in Doppler Radar Data. *Wea. Forecasting*. doi:10.1175/WAF-D-11-00154.1, in press.

Schenkman, A., M. Xue, and A. Shapiro, 2012: Tornadogenesis in a simulated mesovortex within a mesoscale convective system. J. Atmos. Sci. doi:10.1175/JAS-D-12-038.1, in press.

Schneider, R.S., and A.R. Dean, 2008: A comprehensive 5-year severe storm environment climatology for the continental United States. Preprints, *24th Conf. Severe Local Storms*, Savannah, GA, 16A.4.

Schumacher, P.N. and J.M. Boustead, 2011: Mesocyclone evolution associated with varying shear profiles during the 24 June 2003 tornado outbreak. *Wea. Forecasting*, **26**, 808–827.

Sherburn, K.D., and M.D. Parker, 2012: Identifying discriminating environmental features between high shear/low CAPE severe convection and null events. Preprints, *25th Conf. Severe Local Storms*, Nashville, TN, 9.1.

Smith, B.T., R.L. Thompson, J.S. Grams, C. Broyles, and H.E. Brooks, 2012: Convective modes for significant severe thunderstorms in the contiguous United States. Part I: Storm classification and climatology. *Wea. Forecasting*, **27**, 1114–1135.

Smith, T., and K. L. Elmore, 2004: The use of radial velocity derivatives to diagnose rotation and divergence. Preprints, 11th Conf. on Aviation, Range, and Aerospace, Hyannis, MA, Amer. Meteor. Soc., P5.6.

Stumpf, G. J., A. Witt, E.D. Mitchell, P. L. Spencer, J. T. Johnson, M.D. Eilts, K.W. Thomas, and D.W. Burgess, 1998: The National Severe Storms Laboratory Mesocyclone Detection Algorithm for the WSR-88D. *Wea. Forecasting*, **13**, 304–326.

Thompson, R.L., B.T. Smith, J.S. Grams, AR. Dean, and C. Broyles, 2012: Convective modes for significant severe thunderstorms in the contiguous United States. Part II: Supercell and QLCS tornado environments. *Wea. Forecasting*, **27**, 1136–1154.

Trapp, R. J., 1999: Observations of nontornadic low-level mesocyclones and attendant tornadogenesis failure during VORTEX. *Mon. Wea. Rev.*, **127**, 1693–1705.

Trapp, R.J., and M.L. Weisman, 2003: Low-level mesovortices within squall lines and bow echoes. Part II: Their genesis and implications. *Mon. Wea. Rev.*, **131**, 2804–2823.

Trapp, R.J., G.J. Stumpf, and K.L. Manross, 2005: A reassessment of the percentage of tornadic mesocyclones. *Wea. Forecasting*, **20**, 680–687.

Weisman, M.L., and R.J. Trapp, 2003: Low-level mesovortices within squall lines and bow echoes. Part I: Overview and dependence on environmental shear. *Mon. Wea. Rev.*, **131**, 2779–2803.

Wood, V.T., R.A. Brown, and D.W. Burgess, 1996: Duration and movement of mesocyclones associated with southern Great Plains thunderstorms. *Mon. Wea. Rev.*, **124**, 97–101.

Wood, V.T., R.A. Brown, and D. Sirmans, 2001: Technique for improving detection of WSR-88D mesocyclone signatures by increasing angular sampling. *Wea. Forecasting*, **16**, 177–184.

7. FIGURES

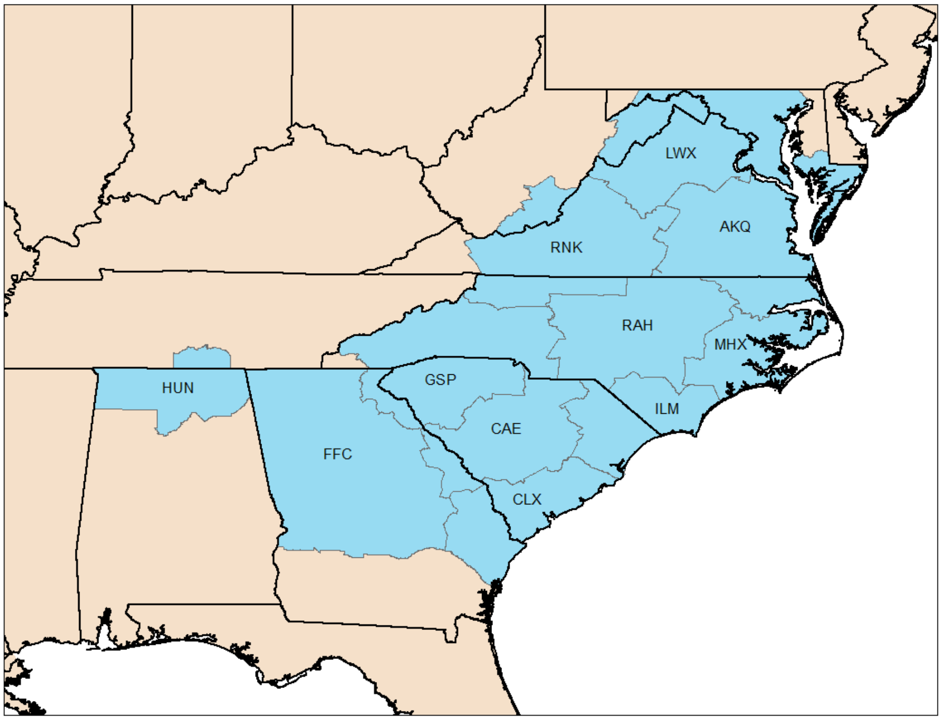

Figure 1: Map of the CWAs that comprised the domain of this study.

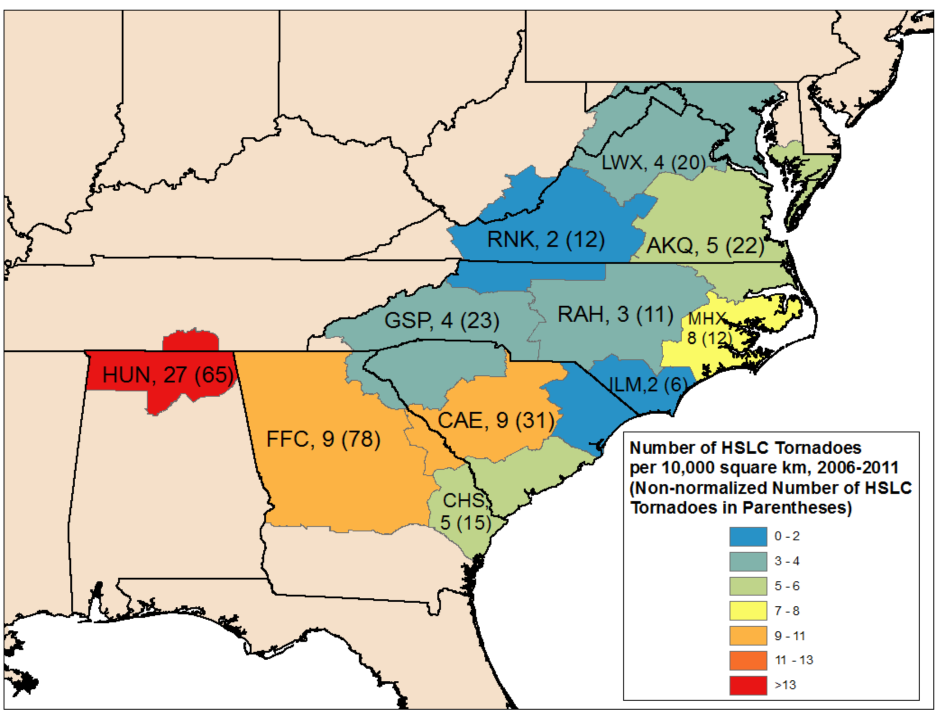

Figure 2: Number of HSLC tornadoes that occurred in each CWA on the days included in this study (between January 2006 and April 2011), normalized by the area of each CWA. Shown in parentheses are the raw (non-normalized) numbers of HSLC tornadoes that occurred in each CWA.

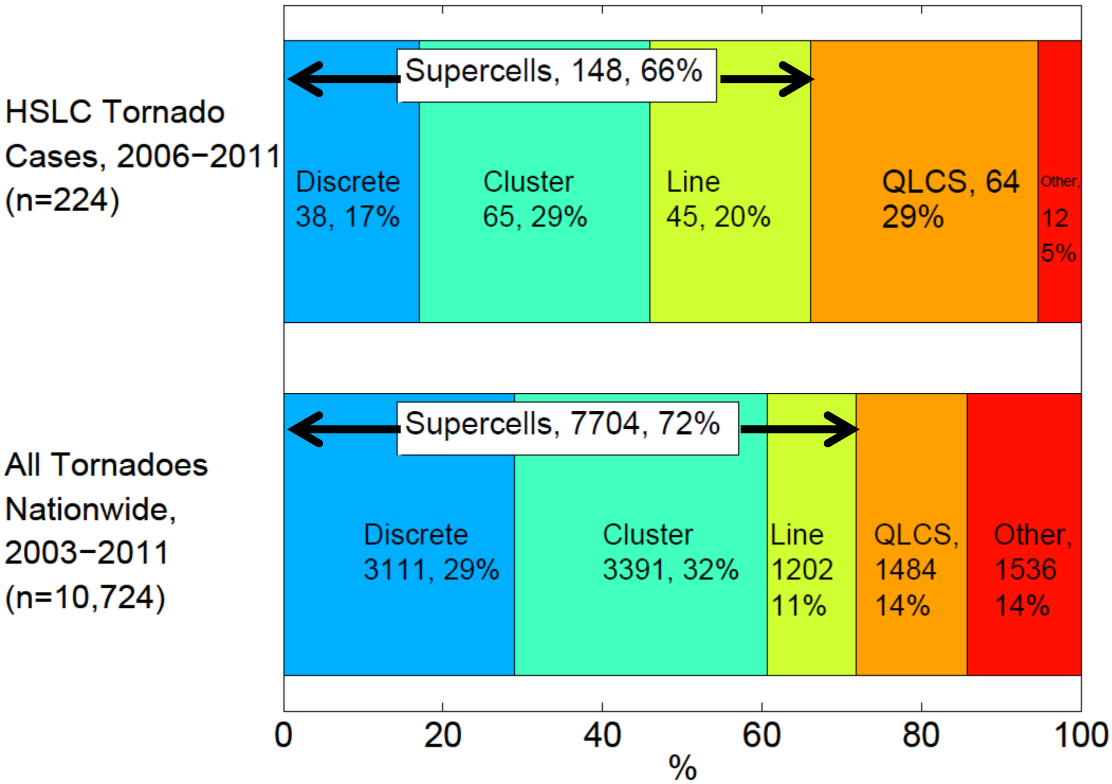

Figure 3: Convective mode distributions for the HSLC tornadoes included in this study (top), and for all tornadoes nationwide that were included in the Smith et al. (2012) convective mode database (bottom). Convective mode classifications are described in the text and in Smith et al. (2012). Percentages are out of 224 for the HSLC tornadoes and out of 10 724 for all tornadoes.

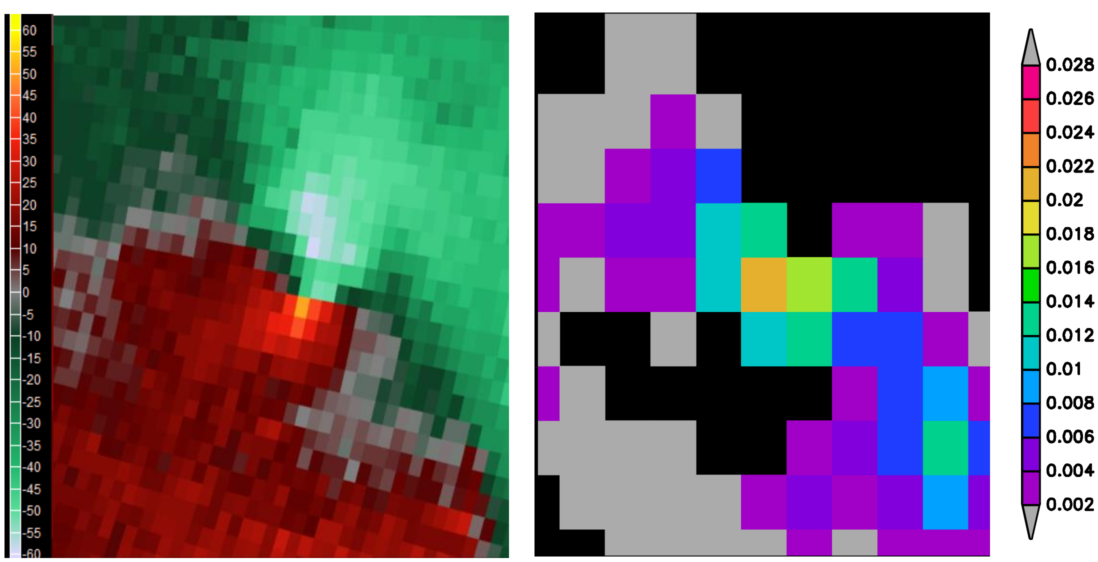

Figure 4: Example plot of radial velocity and azimuthal shear for a vortex, using the same spatial scale for both. The azimuthal shear field shown is originally calculated on a polar grid of same resolution as the velocity data, but then interpolated to a 0.01 degree latitude by 0.01 degree longitude Cartesian grid. The radar is located west-northwest of these images.

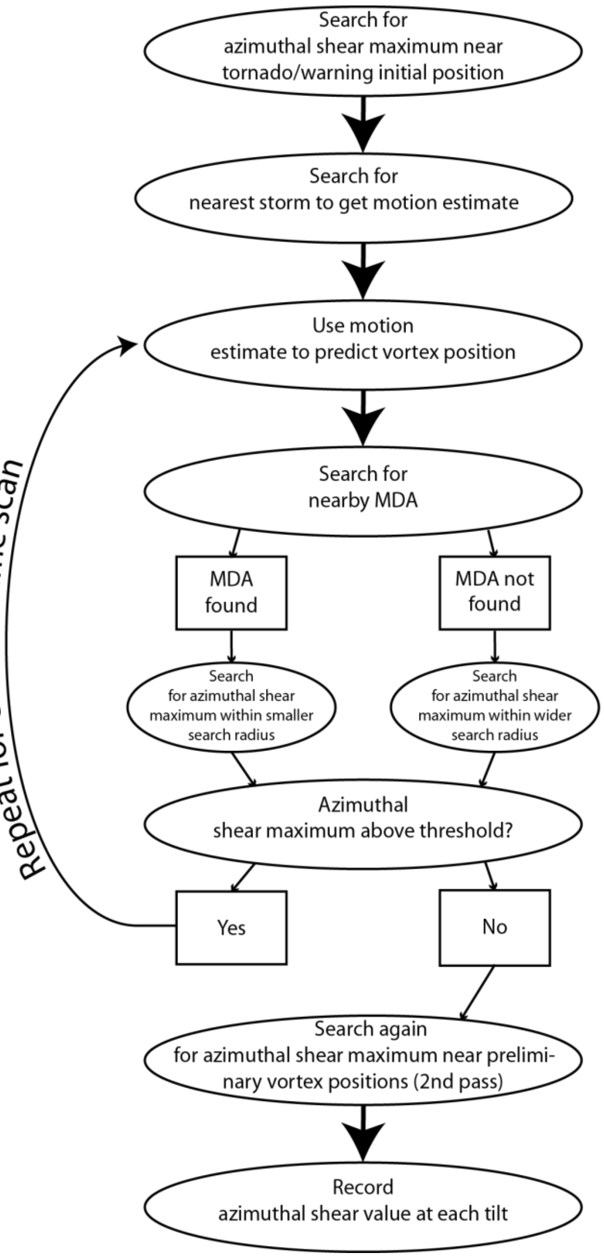

Figure 5: Flow chart for the tracking algorithm that is described in the text.

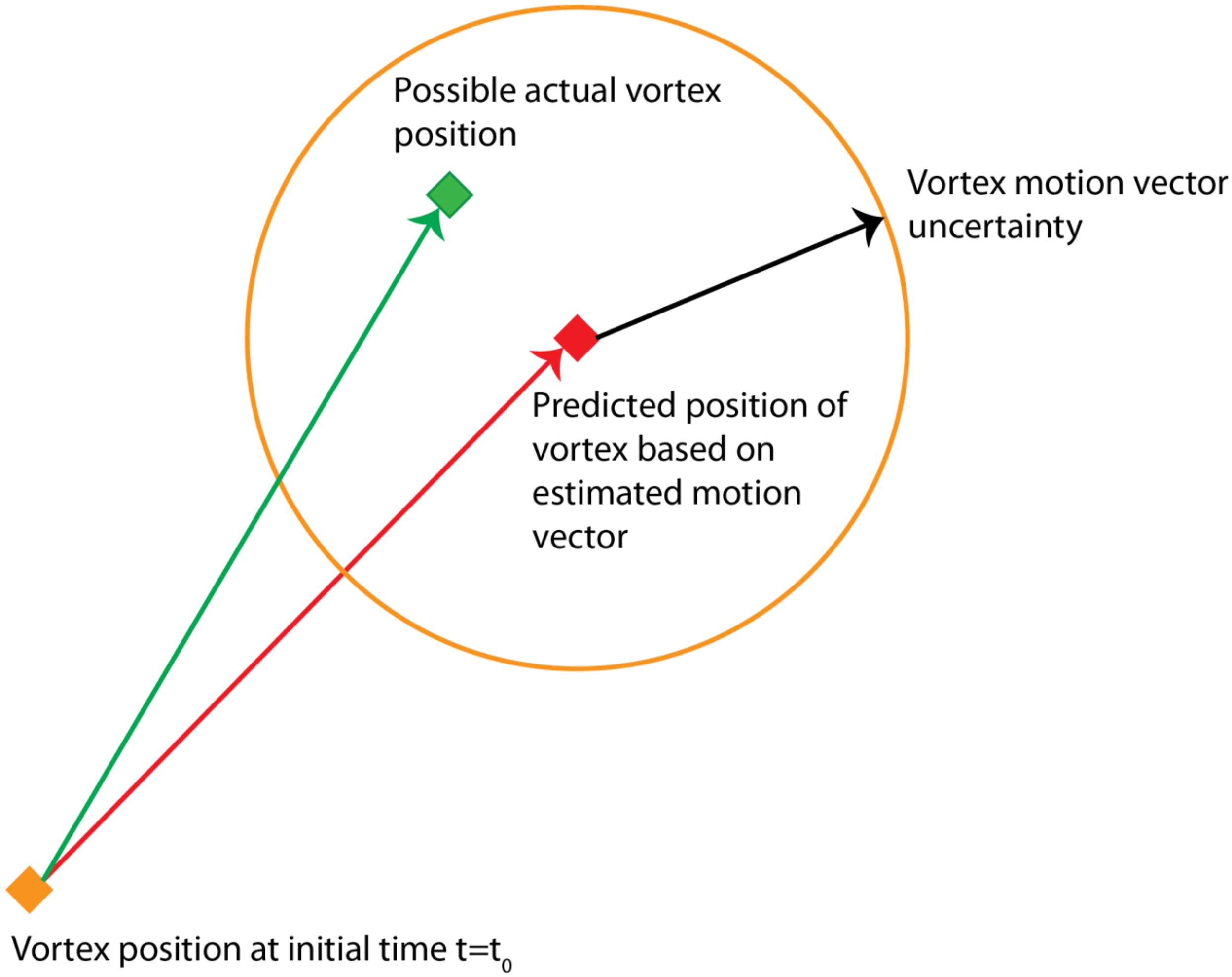

Figure 6: Idealized schematic of tracking algorithm (not to scale). The vortex position, initially found by searching for an azimuthal shear maximum near the tornado touchdown/false alarm warning location, and then found iteratively by repeating the tracking process, is indicated by the orange diamond. A first guess prediction of the vortex is determined based on an estimate of vortex motion (see text for details), which is shown as the red diamond. An estimate of the uncertainty of the vortex motion vector is given by the black arrow, which sweeps out the search radius indicated by the orange circle. The tracking algorithm searches for any MDA-detected mesocyclones within this search radius, and if none are found it searches for the azimuthal shear maximum within this search radius. The green diamond indicates a possible position for the new vortex position.

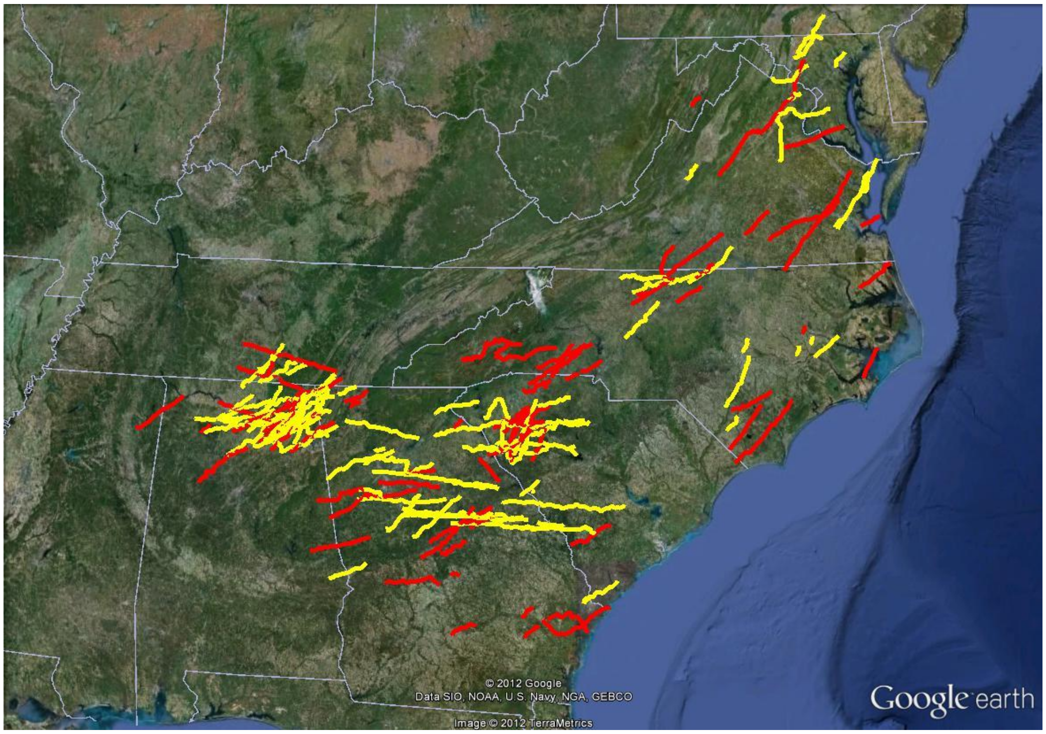

Figure 7: Tracks of the 83 tornadic vortices (yellow) and 84 non-tornadic vortices (red) that were tracked by the tracking algorithm.

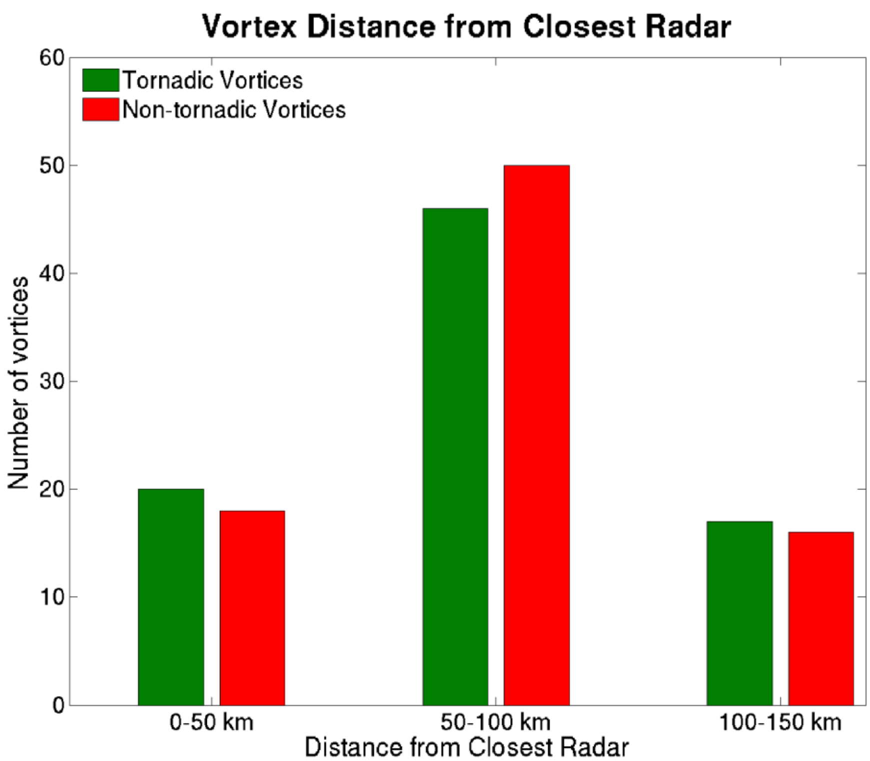

Figure 8: Histogram of vortex distance from the closest radar, using the position of the tornado touchdown for the tornadic vortices, and the position of the false alarm warning for the non-tornadic vortices.

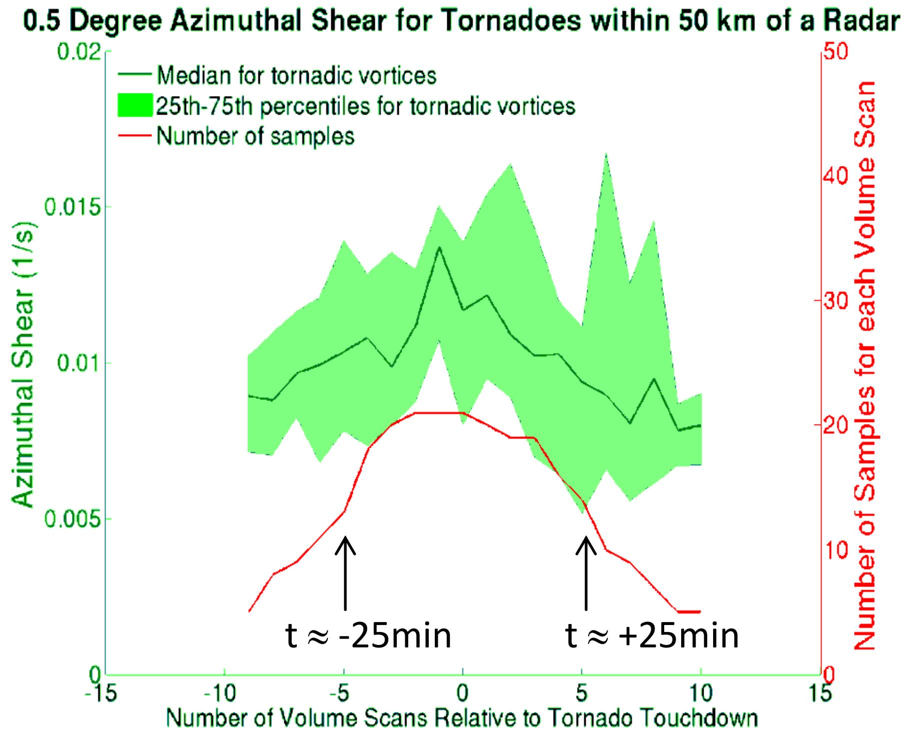

Figure 9: Composite timeseries in a tornado-relative time coordinate system of azimuthal shear at the 0.5 degree elevation scan for tornadic vortices within 50 km of the nearest radar that existed at each volume scan time (green), and number of vortices that existed at each volume scan time relative to tornado touchdown time (red). Azimuthal shear is only plotted if at least five vortices existed at that volume scan time. Annotated is the approximate time of the fifth volume scan before and after tornado touchdown, based on a typical five minute volume scan.

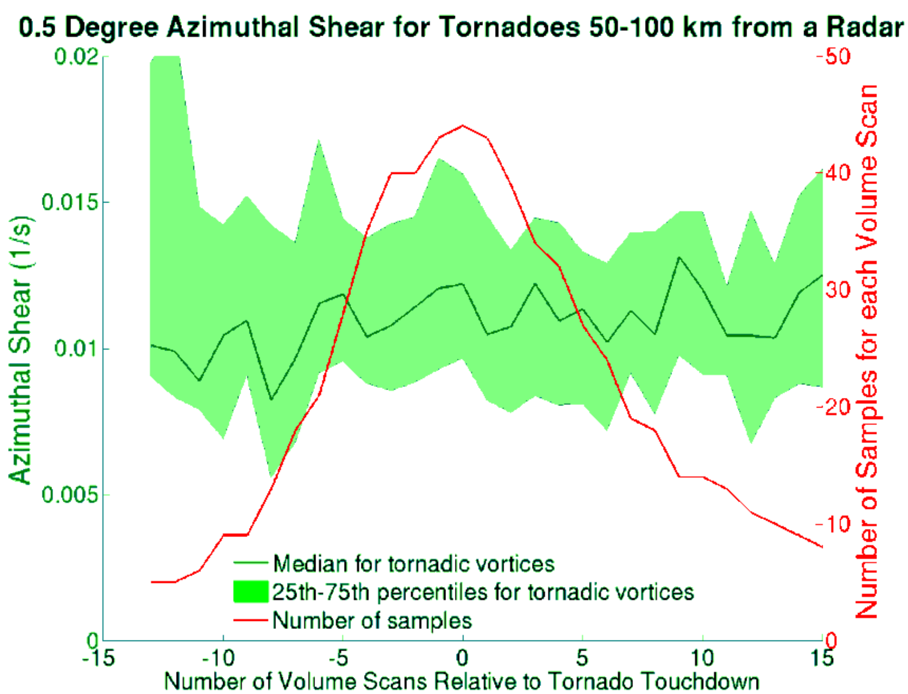

Figure 10: Same as figure 9, but for tornadic vortices between 50 and 100 km from the nearest radar.

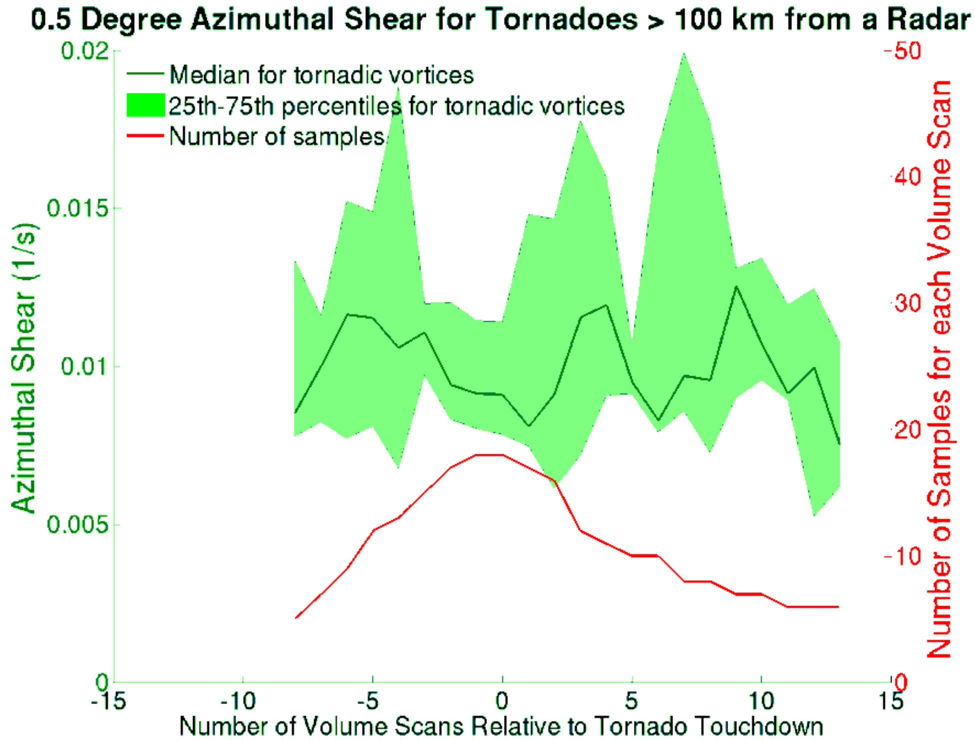

Figure 11: Same as figure 9, but for tornadic vortices greater than 100 km from the nearest radar.

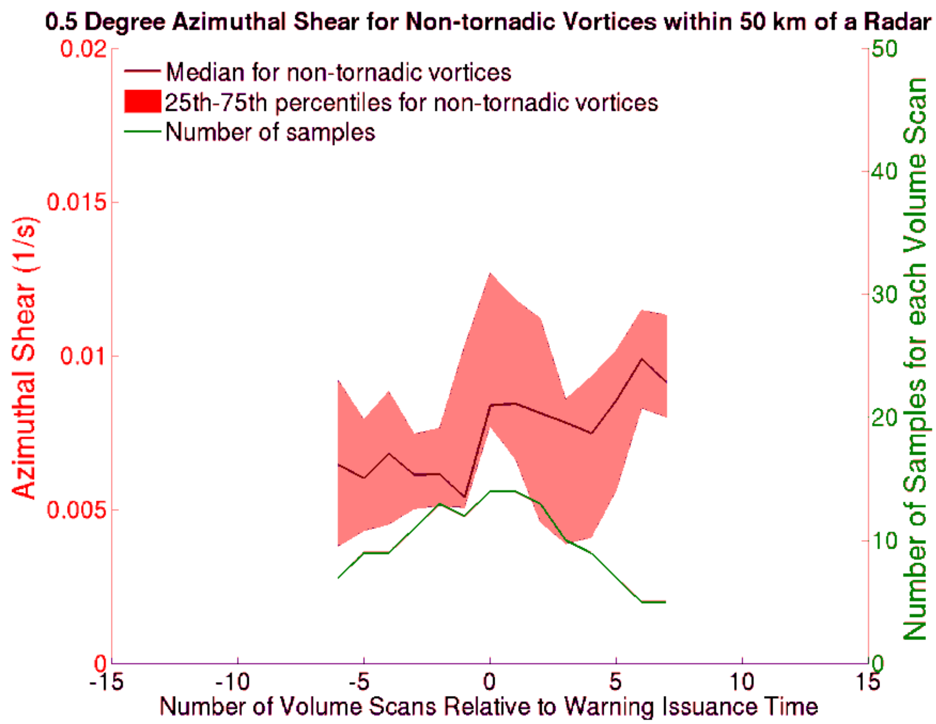

Figure 12: Same as figure 9, but for non-tornadic vortices, and plotted in a false alarm warning-relative time coordinate system. Azimuthal shear is plotted in red, and the number of vortices that existed at each volume scan time is plotted in green.

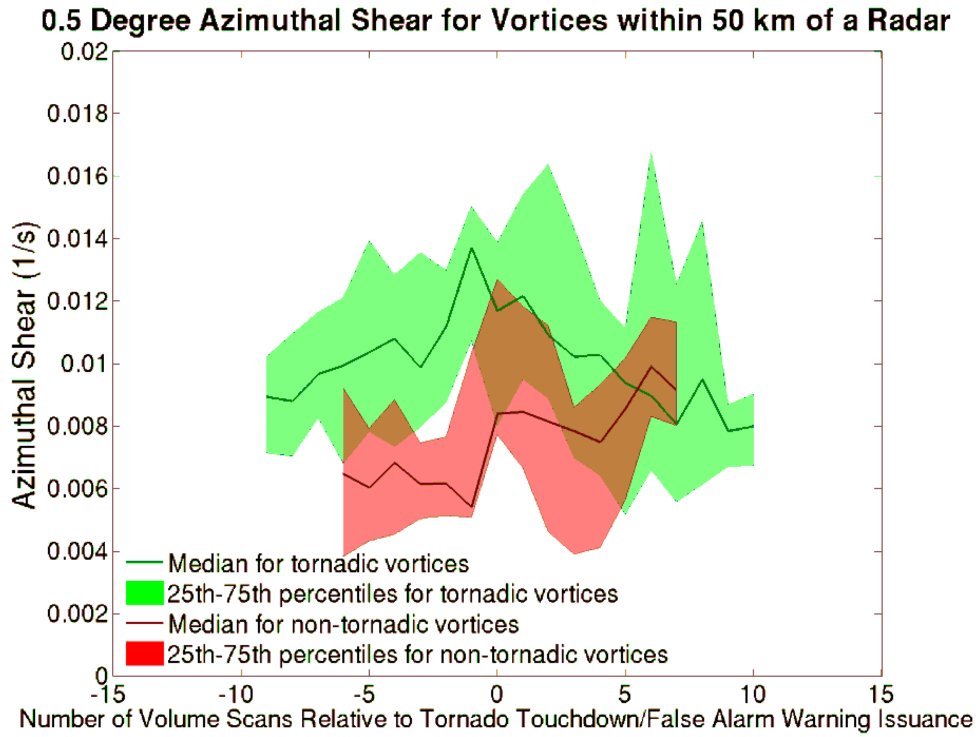

Figure 13: Azimuthal shear at the 0.5 degree elevation scan for tornadic (from Figure 9) and non-tornadic (from Figure 12) vortices within 50 km of the nearest radar.

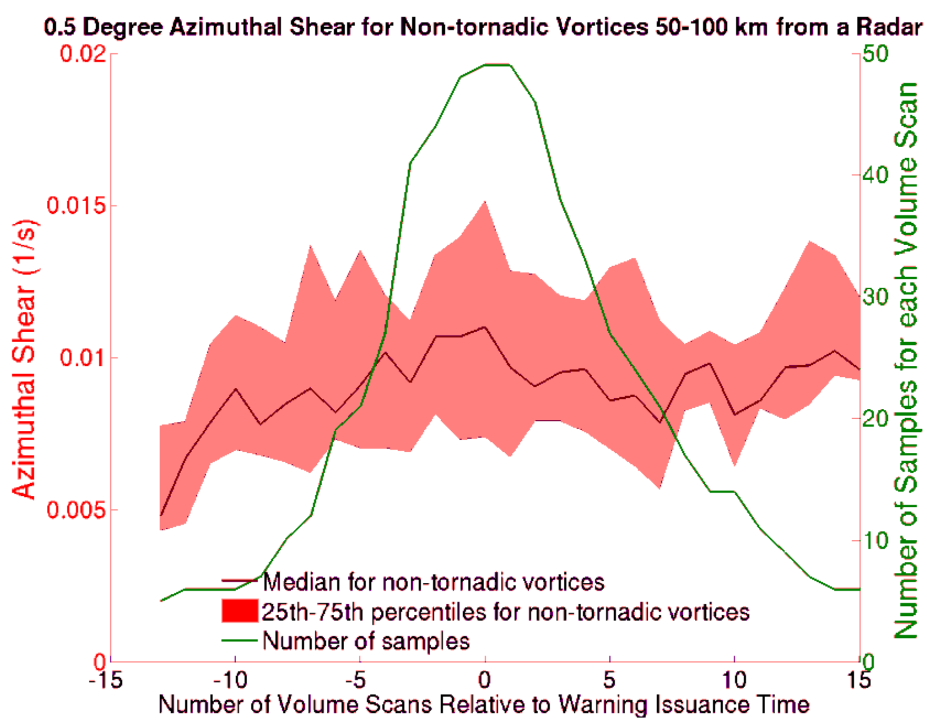

Figure 14: Same as figure 12, but for non-tornadic vortices between 50 and 100 km from the nearest radar.

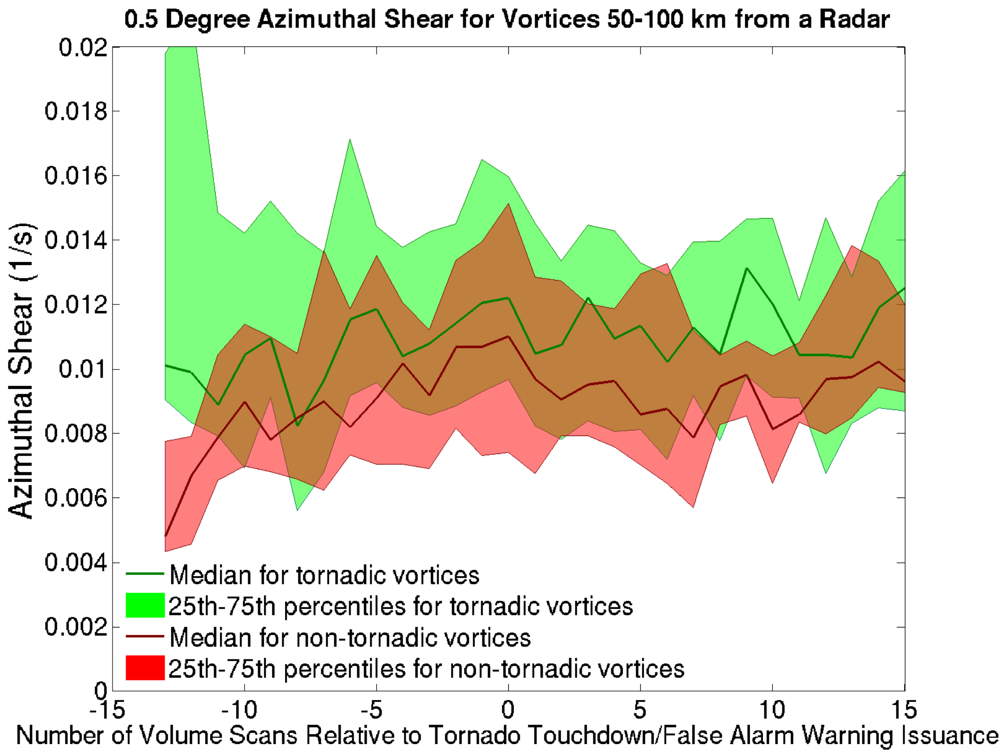

Figure 15: Same as figure 13, but for tornadic and non-tornadic vortices between 50 and 100 km from the nearest radar.

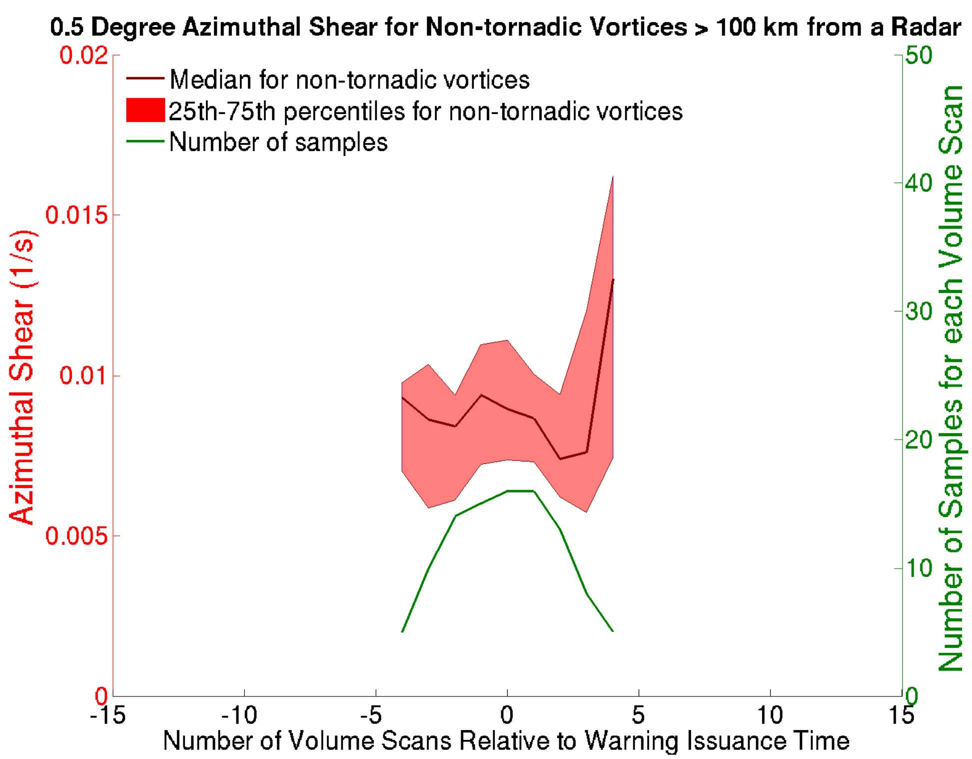

Figure 16: Same as figure 12, but for non-tornadic vortices greater than 100 km from the nearest radar.

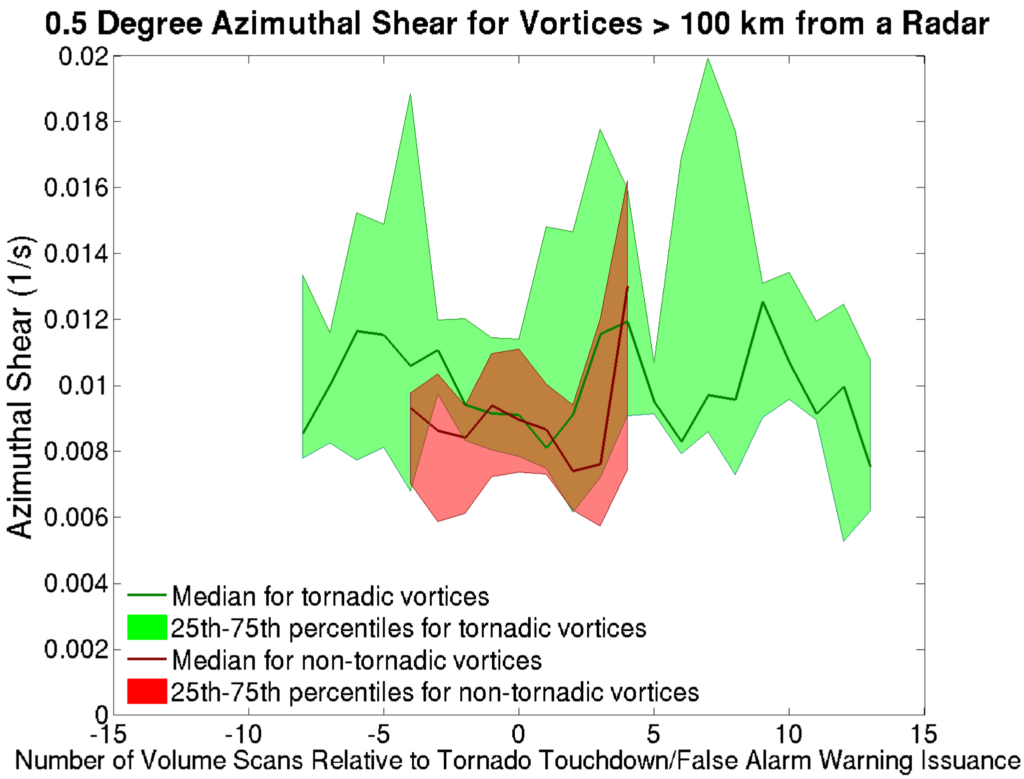

Figure 17: Same as figure 13, but for tornadic and non-tornadic vortices greater than 100 km from the nearest radar.

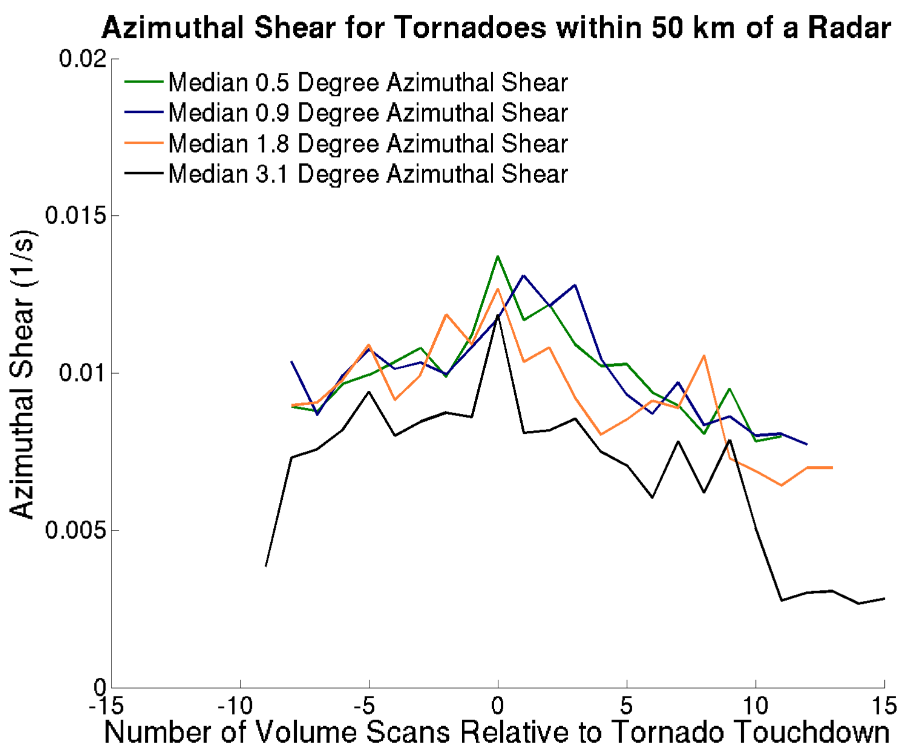

Figure 18: Similar to figure 9, but only median azimuthal shear is plotted, at the lowest six elevation scans for the tornadic vortices that existed at the given elevation scan at the given volume scan time. The 1.3 degree and 2.4 degree elevation scans were omitted for clarity.

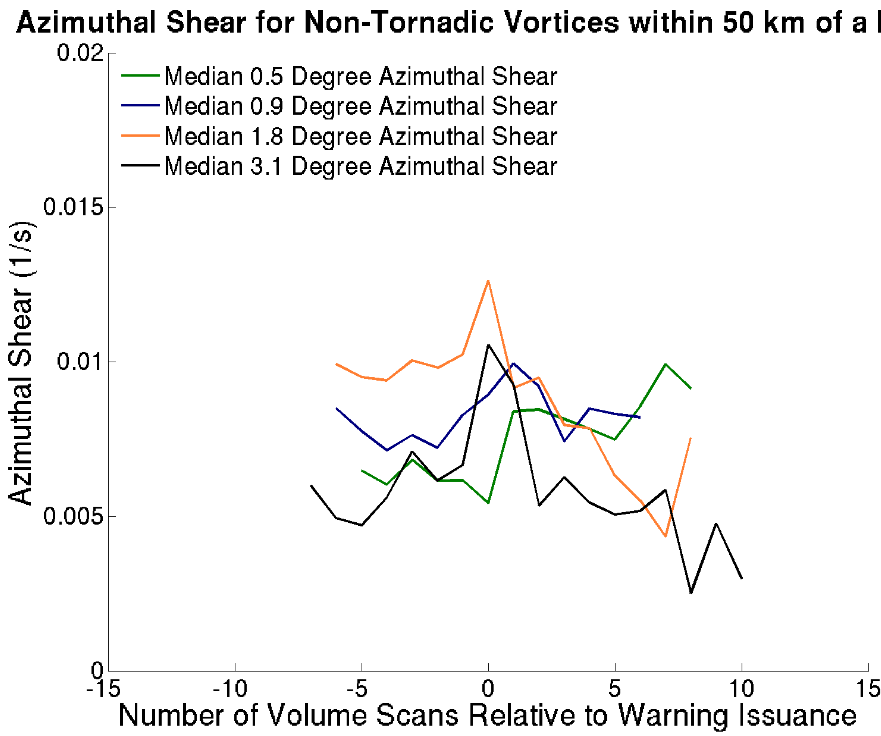

Figure 19: Same as figure 18, but for non-tornadic vortices.

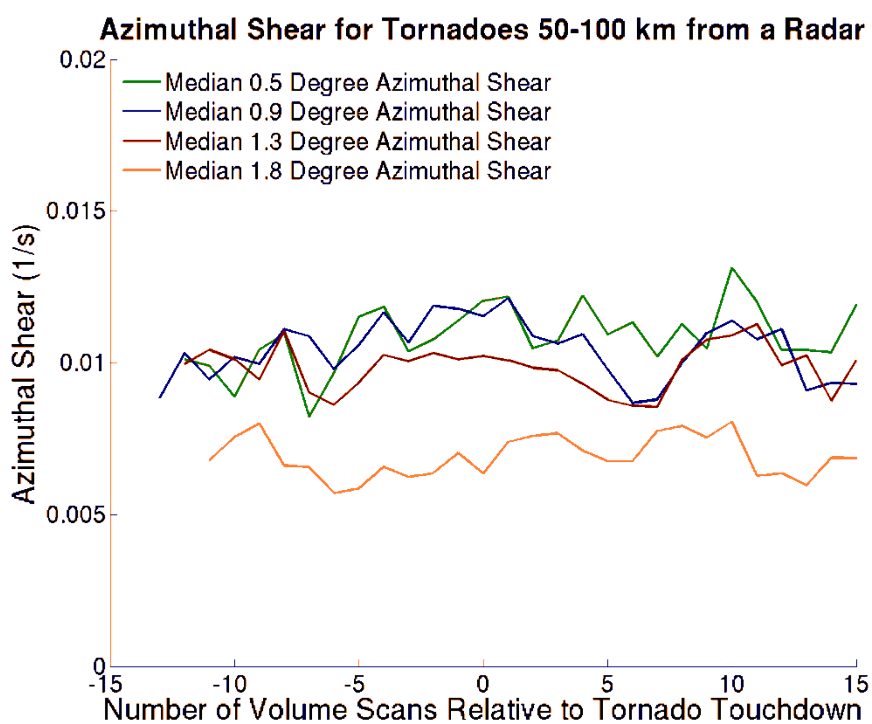

Figure 20: Same as figure 18, but for tornadic vortices between 50 and 100 km from the closest radar. Only the lowest four elevation scans are shown, as median azimuthal shear at higher elevation scans was very weak, and no intermediate elevation scans are omitted.

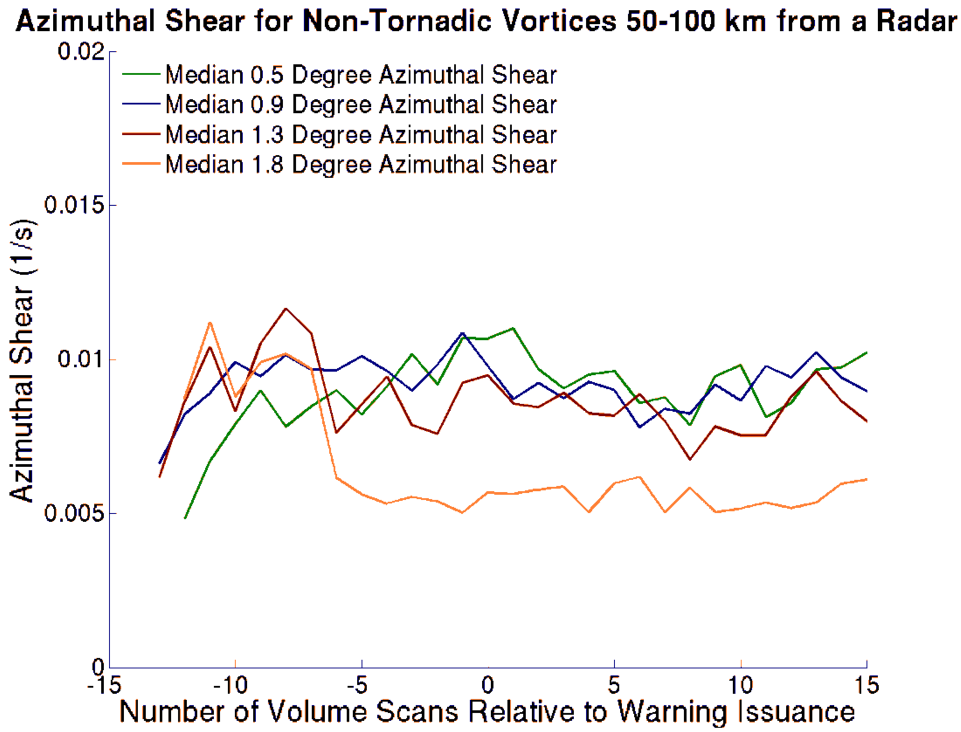

Figure 21: Same as figure 20, but for non-tornadic vortices.